Robotica (2024), **42**, pp. 139–152
doi:10.1017/S026357472300139X

CAMBRIDGE UNIVERSITY PRESS

RESEARCH ARTICLE

The design and kinematic representation of a soft robot in a simulation environment

Hazal Emet[1], Berke Gür[2] and Mehmet İsmet Can Dede[1]

[1]Department of Mechanical Engineering, İzmir Institute of Technology, İzmir, Türkiye and [2]Department of Mechatronics Engineering, Bahçeşehir University, İstanbul, Türkiye
Corresponding author: Mehmet İsmet Can Dede; Email: candede@iyte.edu.tr

Received: 25 January 2023; **Revised:** 5 September 2023; **Accepted:** 28 September 2023;
First published online: 13 November 2023

Keywords: biomimetic robots; novel applications of robotics; unmanned underwater vehicles; serial manipulator design and kinematics; teleoperation; soft robots

Abstract

The increase of human presence in the subsea and seabed environments necessitates the development of more capable and highly dexterous, innovative underwater manipulators. Biomimetic soft-robot arms represent a promising candidate for such manipulation systems. However, the well-known modeling techniques and control theories of traditional rigid robots do not apply to soft robots. The challenges of kinematic and dynamic modeling of soft robots with infinite degrees of freedom require the development of dedicated modeling methods. A novel procedure for representing soft-robotic arms and their motion in a rigid-body simulation environment is proposed in this paper. The proposed procedure relies on the piecewise constant curvature approach to simplify the very complex model of hyper-redundant soft-robotic arms, making it suitable for real-time applications. The proposed method is implemented and verified to be used in model-mediated teleoperation of the soft arms of a biomimetic robotic squid designed for underwater manipulation as a case study.

1. Introduction

Due to the rapid increase in the world population over the next 30 years, it is predicted that the existing natural resources will be insufficient to meet our daily needs in critical areas such as food and energy [1]. Realistic solutions proposed for this rapidly approaching resource crisis include increasing resource utilization, reducing waste, and improving recycling efficiency. In addition to these solutions, the effective and sustainable exploitation of the relatively untapped marine environment appears as another viable remedy.

It is envisioned that the subsea environment will be utilized and exploited much more effectively for food supply, energy production (both from traditional fossil fuels and renewable resources), and infrastructure construction in the near future. It is possible to expand the above list of underwater activities to include mining of valuable and rare metals, minerals, gas hydrates, search and rescue operations, object extraction and retrieval, underwater archeology, geology, biology, ecology, oceanography studies, bio-fuel production, and military applications. Furthermore, it is becoming a necessity to carry out these subsea activities in even deeper waters, away from the coasts, and in dexterous and safe physical interaction with natural or artificial underwater structures.

However, the underwater environment is not suitable for humans to live or engage in any prolonged activity. Therefore, most underwater and seabed activities are delegated to unmanned platforms. Although the worldwide fleet of unmanned submersible robots is growing rapidly, with the expansion of the application areas and the diversification of the tasks expected to be performed, current underwater robot designs will not be sufficient to meet the operational demands, in particular, in terms of

underwater intervention [2]. To overcome this deficiency, there is a strong and urgent requirement to develop underwater robots with advanced manipulation and intervention capabilities.

Biomimetic robots may operate and manipulate objects with complex abilities, expanding the range of applications beyond what is possible with traditional robots. Many bioinspired soft robot designs are influenced by animals living underwater like the octopus. The OctArm [3], an octopus-like soft robot, mimicked the suction and grasping characteristics of octopus' tentacles. Another octopus-like robot, Air-Octor [4], has independently controlled multi-sections and the capability to bend and extend its tentacles. The crawling motion of biological octopuses, whose motion style requires six arms and two legs in its nature, is mimicked by an eight-arm octopus-like robot [5]. In ref. [6], another octopus-like robot composed of completely soft materials, including its body, is presented. A squid robot, the Squidbot [7], with improved maneuverability and movement capability using jet pulses, was recently introduced.

Approaches that define the robotic arm in finite number of degrees of freedom are necessary to model and study soft robots in rigid-body simulation environments. To represent the motion of the soft-robotic arms in these rigid-body simulation environments, a novel modeling framework is required due to the inadequacy of the traditional rigid-body modeling approaches. This modeling framework must follow the same standards of accuracy and computational efficiency as traditional rigid-body robot models. Various modeling methods for soft robots have been developed. Among these, Piecewise Constant Curvature (PCC) [8–11], continuum Cosserat [12–14], and finite element method (FEM) [15–17] techniques are the ones that are most frequently used. The PCC approach simplifies and represents the soft-robotic arm model as a finite set of mutually tangent constant curvature arcs defined by three parameters: arc length (ℓ), angle through which the arc bends (θ), and angle of the plane containing the arc (ϕ) [18]. This simplification results in a significant decrease in the number of variables required. The continuum Cosserat approach represents the soft-robotic arm with an infinite number of small sections, similar to micro solids. Contrary to the PCC method, the continuum Cosserat method does not discretize the soft robot into sections that can be represented as rigid-body manipulators. Although this method yields highly accurate results, the obtained equations to manipulate the soft robot are computationally expensive and more challenging from the control point of view [19]. The FEM modeling approach is the most accurate and computationally expensive one of these three modeling approaches [15, 17, 20]. Furthermore, the preprocessing stage of FEM, which is necessary for modeling, is more extensive and time-consuming compared to the other two methods, thereby also increasing the required human effort.

Programming environments tailored for rigid-body manipulators have dominated the industry for years, establishing themselves as the preeminent solutions with large-scale applications. There has been a recent emergence of soft-robot-specific programs, which are mostly built upon FEM-based methods. Nonetheless, due to their limited efficiency in terms of computation time, these programs are not preferred for the purposes of our research. Our objective in this study is to formulate an alternative method using PCC approach, which necessitates lower computational costs, that can still yield satisfactory results. Additionally, within the chosen rigid-body simulation environment, the availability of interfaces with external devices (e.g. haptic devices, data acquisition cards) enables the seamless integration of the generated soft-robot model with such hardware.

Due to its computational efficiency, the PCC approach is the most popular modeling strategy for soft robotics [8] and is adopted in this work for the same reason. This paper presents a procedure to virtually represent the soft robot arms in MATLAB Simulink graphical programing environment. The soft arms are defined as discrete multi-section rigid-body manipulators using the PCC approach. In order to model and simulate a soft robot and its desired characteristics such as bending and elongating, the requirements of that environment should be considered to adopt the suitable approach. The procedure defined in this paper explains such a method and is implemented on a biomimetic squid robot to represent its soft robot arms.

The primary contribution of this paper is the introduction of a novel method for simulating soft robots in an environment that is developed for rigid-body models. The PCC approach is implemented to represent the soft-robotic arms in this environment. The proposed method can reduce the computational cost

https://doi.org/10.1017/S026357472300139X Published online by Cambridge University Press

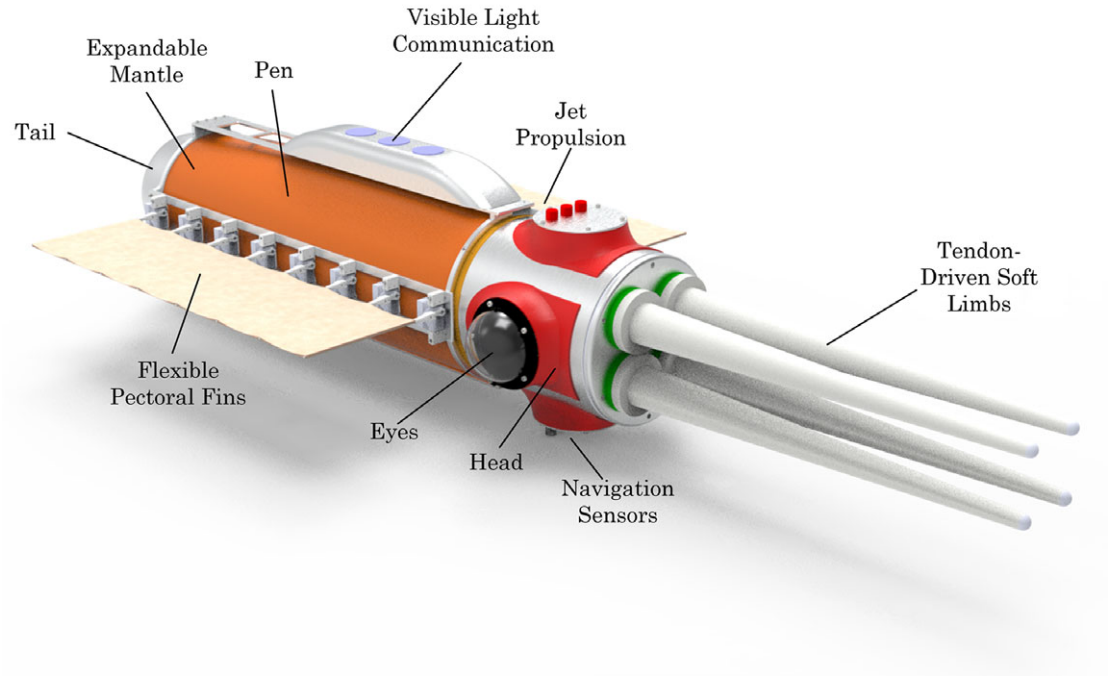

Figure 1. *A rendering of the production-ready 3-D solid model of URSULA highlighting key design aspects.*

(in particular, for simultaneous simulation of multiple soft limbs) compared to FEM-based methods. This alternative approach may be useful in applications that require real-time operation without considerable loss in accuracy. The main assumption in this study is that the pose of the soft robot is available at all times.

The work presented in this paper is conducted as an initial step toward developing a teleoperation method for an underwater soft biomimetic squid robot. The aimed master-slave teleoperation control method is selected to be a model-mediated teleoperation strategy [21]. In this teleoperation system, a replica of the slave system is re-generated at the master side as a representation of the slave environment in simulation. This is required due to the limited bandwidth provided by wireless underwater communication protocols such as acoustic or visible-light communication between the master and the slave. Consequently, on the master side, a virtual reality simulation of the slave model is to be run in real time. As a result of this requirement, the soft robot representation of the slave system's soft arms has to run in a computationally efficient way. In our case, the slave system is composed of multiple soft robot arms.

2. Robotic squid for underwater manipulation and intervention

In this section, the squid-inspired, biomimetic robot platform designed for dexterous underwater manipulation and seabed intervention (dubbed Project URSULA) is introduced. Design details of the soft-robotic limbs hosted by this robotic platform are also presented.

2.1. Design of the proposed biomimetic underwater robot

Inspired by the common squid and cuttlefish, URSULA is comprised of 7 main body parts: (1) soft limbs, (2) head, (3) pen, (4) expandable mantle, (5) tail, (6) visible-light communication system, and (7) flexible pectoral fins (see Fig. 1). The overall system length (excluding the limbs) is less than 1200 mm

https://doi.org/10.1017/S026357472300139X Published online by Cambridge University Press

while the limbs are 600 mm long. The largest diameter is 250 mm at the head. The total dry weight of the URSULA is around 30 kg, and the robot is designed to be slightly positively buoyant. The head, pen, and tail form the rigid, watertight components of the main body. Tendon-driven soft limbs are attached to the head. The head houses the tendon actuators as well as several navigation sensors. The pen bridges the head to the tail, functioning as an internal shell that hosts the electronics housing and batteries. The connector for the (optional) umbilical cable or tether and other waterproof connections are located at the tail. The port and starboard pectoral fins (each grouped into three sections) form the main actuation system of the robot and are attached to the two rails on the port and starboard sides that run along the length of the pen, outside of the mantle. These lateral rails are complemented with a pair of identical dorsal and ventral rails, which are used to attach several navigational sensors and the visible-light communication system. The visible-light communication system, in the form of a dorsal fin, provides a wireless communication interface required for the haptic teleoperation of the limbs. The jet propulsion system is designated as the secondary propulsion system and is located toward the front part of the pen, inside of the expandable mantle. Sea water is pumped into the double-walled soft mantle. This causes the mantle to expand inwards increasing water pressure between the mantle and pen. When sufficient water pressure is obtained, a solenoid valve is opened forcing the water out through a steerable nozzle. A 3-D render of the robot is presented in Fig. 1.

Although the initial design has only four limbs, future designs may incorporate more. A sonar is expected to be integrated, primarily to complement the existing navigation sensors in underwater SLAM-based navigation. The head will also host a 3-D stereo vision system for teleoperation and generating a virtual 3-D model of the surrounding environment. The information gathered from this camera will be used to regenerate obstacles in the master side of the teleoperation system. There is an additional camera in one of the limbs to capture views close to the tip of the limbs.

2.2. Soft-robotic limb design

The primary motivation behind URSULA was to develop a robot that can dexterously interact with the underwater environment. Therefore, the soft-robotic limbs are the most crucial subsystem of the robot. In the current design, the robot has four soft, tendon-actuated robotic limbs protruding from the head. Two of these limbs are designated as arms and are designed to provide functionality such as reaching, gripping, and pulling to perform manipulation tasks such as palpation, grasping, and retrieval. The remaining two limbs are designated as tentacles. These tentacles host an underwater camera and lighting system embedded at their distal ends. The camera system supplements the on-board 3-D vision system for visual feedback assisted teleoperation of the limbs as well as environment mapping. The motion of the light tentacle is synchronized with the camera tentacle to effectively illuminate the workspace of the arms. The tentacles are fully functional limbs and can also be used for other manipulation tasks such as anchoring the robot. The breakdown of the four limbs is grasper, palpation, camera, and light arms. The grasper arm is designated to be used in tasks such as holding or picking an intervened object. The palpation arm's task is assigned as palping motion. A force sensor is mounted on the end of the limb. The manipulation of the palpation arm is similar to the manipulation of the grasper arm. The palping motion is achieved by the limited elongation of the soft arm. Both the camera and light arms are used to provide appropriate visual feedback to the operator.

Inspired by squid and cuttlefish tentacles, the hyper-redundant soft robot limbs are molded from Smooth-On Ecoflex 00-30 elastomer material. Ecoflex is almost neutrally buoyant in water with a mass density of 1070 kg/m^3. It has Young's modulus of 69 kPa and tensile strength of 1.38 MPa. Poisson's ratio is assumed to be ∼0.5 (nearly incompressible) since the bulk modulus of rubber is much larger compared to the modulus of rigidity. Owing to the highly elastic, soft material used in their construction, the robotic limbs can safely interact with the fragile environment in tasks, such as palping and grasping, and handle delicate payloads and underwater objects.

The limbs are designed as thin and slender frustums with a length of 600 mm. Due to the size limitations of URSULA, the diameter at the base of the limbs (where the limbs are attached to the head) is

https://doi.org/10.1017/S026357472300139X Published online by Cambridge University Press

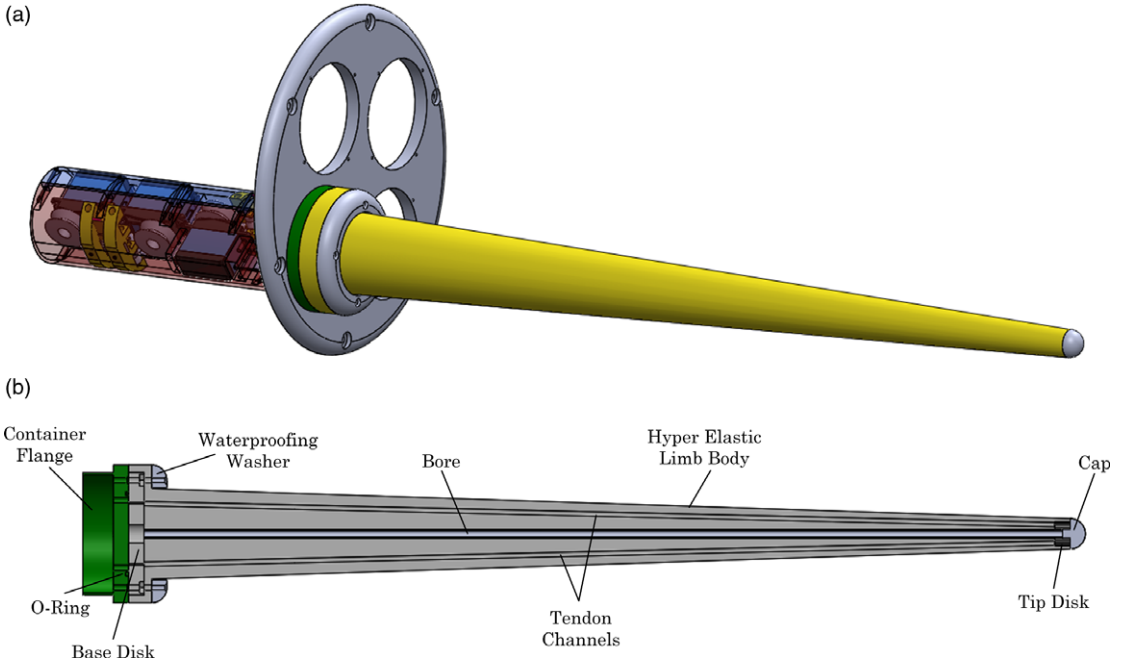

Figure 2. *(a) The 3-D solid model of the limb system (showing only a single limb) and (b) the cross-sectional cut of a robotic limb labeled with the main parts.*

60 mm and reduces linearly to 20 mm at the tip. The limbs are actuated by a set of tendons channeled longitudinally through the body of the limbs (see Fig. 2b). Although 3-tendon configurations are investigated with promising initial results, a 4-tendon configuration is preferred for the preliminary design due to the simpler shape control strategies associated with the decoupling of the tendon actuation. In fact, more tendons (e.g., 6 tendons) can be used to increase the control accuracy. However, there is a tradeoff between the complexity of the actuation-tendon number and system size. In order to fit the actuation systems of the four limbs into the confined space of the head, the number of actuators and tendons per arm is limited to four, sacrificing some control accuracy. Thin channels made from soft silicone tubes are used to guide the tendons along the length of the limbs and provide a protective sheath to prevent the tearing of the soft limbs. The tendons are anchored to a rigid disk embedded into the limb at the tip and are connected to electro-mechanical actuators at the other end. Another rigid disk embedded at the base of the limb serves as the mechanical interface to 80 mm diameter flanges used to connect the limbs to the bow plate of the head. Aside from the tendon channels, another larger silicone tube is placed centrally along the spine of the arm and serves as the cable channel for the camera and lighting system. The solid model of the limbs is provided in Fig. 2a.

3. Discretized soft robot arm design and modeling approach in rigid-body simulation environment

A rigid-body simulation environment is used for soft robot modeling to minimize the computational cost. Consequently, a suitable procedure is required to represent the soft robot characteristics in a virtual environment that is developed for rigid-body systems. A soft robot arm can be composed of multiple independently controllable segments. In this procedure, the motion of each segment of the soft arm is represented as an RRP serial manipulator's motion, where R and P denote revolute and prismatic joints, respectively. Segments are then represented with discretized sections consisting of rigid-body

https://doi.org/10.1017/S026357472300139X Published online by Cambridge University Press

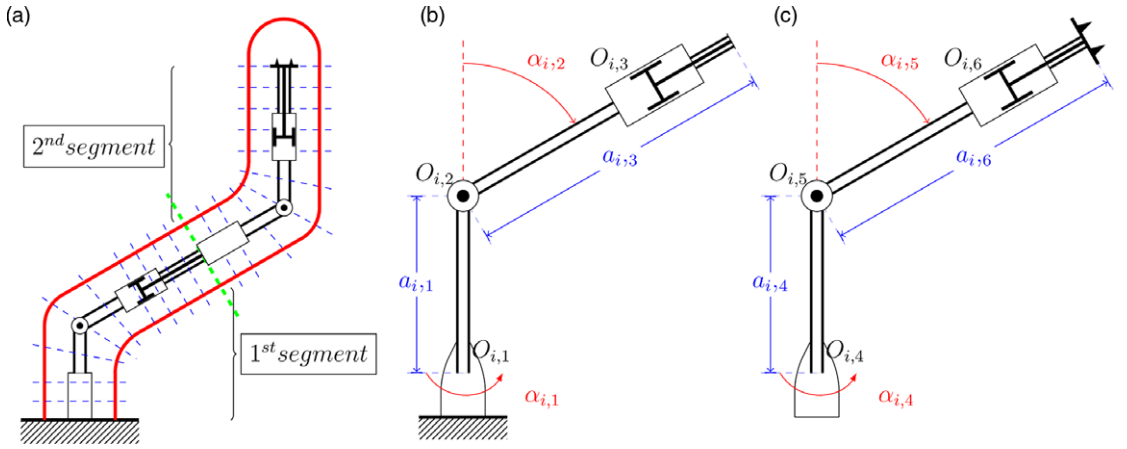

Figure 3. *Kinematic sketches of the robot arms: (a) Representation of soft robot arm; (b) Soft robot arm first segment; (c) Soft robot arm second segment.*

manipulators based on the RRP manipulator's joint motion variables. The procedure is broken down into six steps as follows:

1. Define the motion of each segment of the soft robot arm based on an RRP manipulator's joint motion.
2. Define a curve equation to represent the shape of each segment of the soft robot arm.
3. Relate the RRP manipulator's joint motions to the selected curve equation's parameters.
4. Discretize the resultant curve equation to N sections with equal lengths.
5. Use these discretized pieces' coordinates to define a small-sized RRP manipulator for each discretized piece.
6. Assemble N number of visual models representing small-sized RRP manipulators on top of each other to form the visual representation of one segment of the soft robot arm.

3.1. Kinematic modeling

The robot arm, as presented in Fig. 3, can only have one or two segments mounted on top of each other. In Fig. 3a, the mounting location of two segments on top of each other is indicated by the green dashed line. Here, each segment is chosen to be discretized into 10 pieces, $N = 10$. Each segment is indicated by the thin dashed blue lines in Fig. 3a. Each section is composed of a spherical arm with RRP serial manipulator architecture. The kinematic sketches of RRP manipulators representing the motion of each segment are presented in Fig. 3b and c. Each segment architecture is created with zero offset for $a_{i,1}$ and $a_{i,4}$ parameters; hence, this architecture represents the spherical coordinates with variables $\{\alpha_{i,1}, \alpha_{i,2}, a_{i,3}\}$ for segment 1 and $\{\alpha_{i,4}, \alpha_{i,5}, a_{i,6}\}$ for segment 2. The offsets of robot arms are represented by a parameters, and α parameters represent the R joint angles of the RRP manipulator representing a segment of a soft arm.

In our case, there are four soft robot arms with one and two segments: grasper and palpation arms have two segments, and camera and light arms have one segment. The $\bar{\alpha}$ and $\bar{a}$ column matrices are defined as $\bar{\alpha} = [\bar{\alpha}_g^T\ \bar{\alpha}_p^T\ \bar{\alpha}_c^T\ \bar{\alpha}_l^T]^T$, $\bar{a} = [\bar{a}_g^T\ \bar{a}_p^T\ \bar{a}_c^T\ \bar{a}_l^T]^T$, where $\bar{\alpha}_i = [\alpha_{i,1}\ \alpha_{i,2}\ \alpha_{i,3}\ \alpha_{i,4}\ \alpha_{i,5}\ \alpha_{i,6}]^T$, $\bar{a}_i = [a_{i,1}\ a_{i,2}\ a_{i,3}\ a_{i,4}\ a_{i,5}\ a_{i,6}]^T$ and $i = g, p, c, l$ define the arm type as grasper, palpation, camera, and light arms of the slave robot. The $\alpha_{i,4}, \alpha_{i,5}, \alpha_{i,6}$ and $a_{i,4}, a_{i,5}, a_{i,6}$ parameters are simply not valid for soft robot arms with only one segment.

https://doi.org/10.1017/S026357472300139X Published online by Cambridge University Press

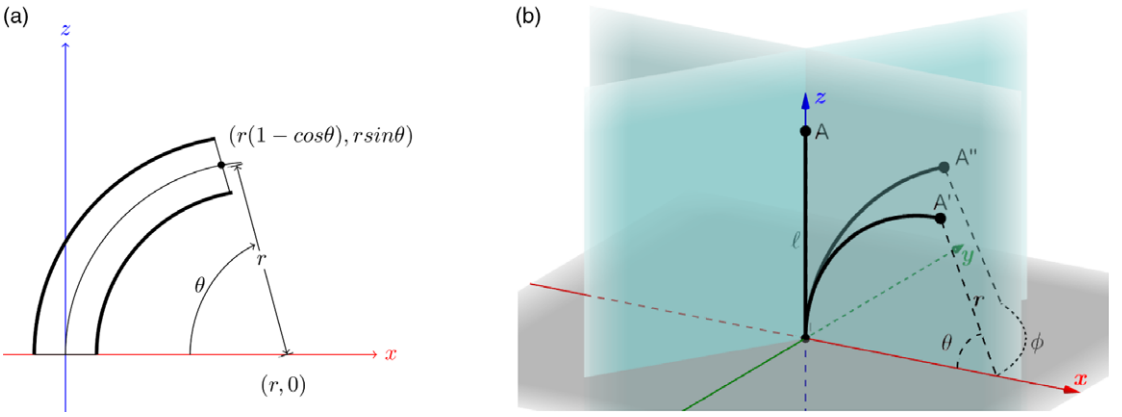

Figure 4. *PCC approach: (a) $\phi = 0$, arc in the x-z plane; (b) $\phi \neq 0$ (adapted from [18]).*

3.2. Modeling the robot arms with piecewise constant curvature approach

The mathematical model of a segment of the virtual robot arms is derived using the PCC approach, described in Fig. 4. Three parameters are required to model the soft arms: the arc length (ℓ), the angle (θ) through which the arc bends, and the angle (ϕ) defining the relative motion of the plane containing the arc about the z-axis.

The curve defined in the PCC approach is discretized into 10 pieces with equal lengths, which are represented as sections. A curve equation is selected to mimic the soft robot motion characteristics. In this work, a quarter of a circle is selected as the curve. The quarter of a circle-based curve equations, presented in Eqs. (1)–(6), are used to derive the PCC parameters for a two-segment soft robot arm. If the soft robot arm has one segment, only the Eqs. (1)–(3) are used. In Eqs. (1)–(6), PCC parameters are related to the kinematic model parameters presented in Section 3.1 as follows: $\phi = (\alpha_{i,1}, \alpha_{i,4})$ and $\theta = (\alpha_{i,2}, \alpha_{i,5})$ and $x_{e,1}$, $z_{e,1}$, $x_{e,2}$, and $z_{e,2}$ parameters define the tip-point position of the soft robot arm in the x, y, and z-axes. Here, r_1 and r_2 define the arc radii for the first and second segments based on θ and ℓ values for the respective segment where $\ell = (a_{i,3}, a_{i,6})$, $r_1 = a_{i,3}/\alpha_{i,2}$, and $r_2 = a_{i,6}/\alpha_{i,5}$ for segment 1 and 2, respectively. The initial position of the segments is obtained when $\theta = 0^\circ$ and $\phi = 0^\circ$. In this condition, the segments are in their initial lengths $a_{i,3} = a_{i,6} = 300$ mm for a two-segment arm and $a_{i,3} = 600$ mm for a single-segment arm.

$$x_{e,1} = (-r_1 \cos(\alpha_{i,2}) + r_1) \cdot \cos(\alpha_{i,1}) \tag{1}$$

$$y_{e,1} = (-r_1 \cos(\alpha_{i,2}) + r_1) \cdot \sin(\alpha_{i,1}) \tag{2}$$

$$z_{e,1} = r_1 \sin(\alpha_{i,2}) \tag{3}$$

$$x_{e,2} = (-r_2 \cos(\alpha_{i,5}) + r_2) \cdot \cos(\alpha_{i,4}) \tag{4}$$

$$y_{e,2} = (-r_2 \cos(\alpha_{i,5}) + r_2) \cdot \sin(\alpha_{i,4}) \tag{5}$$

$$z_{e,2} = r_2 \sin(\alpha_{i,5}) \tag{6}$$

The initial position of the soft arms is defined in the $+z$-axis for this work with $\theta = 0^\circ$ and $\phi = 0^\circ$. Given an arc that cuts through θ degrees extending from the origin tangent to the z-axis and bending about the y-axis, the angle between the z-axis and a line connecting the origin to the arc tip is $\theta/2$, described in Fig. 5. To ease the implementation of the PCC approach, the bending angle of the arc, θ, is defined from the initial position of the arms as $\theta/2$. Unit vectors along the x and z-axes on the base

https://doi.org/10.1017/S026357472300139X Published online by Cambridge University Press

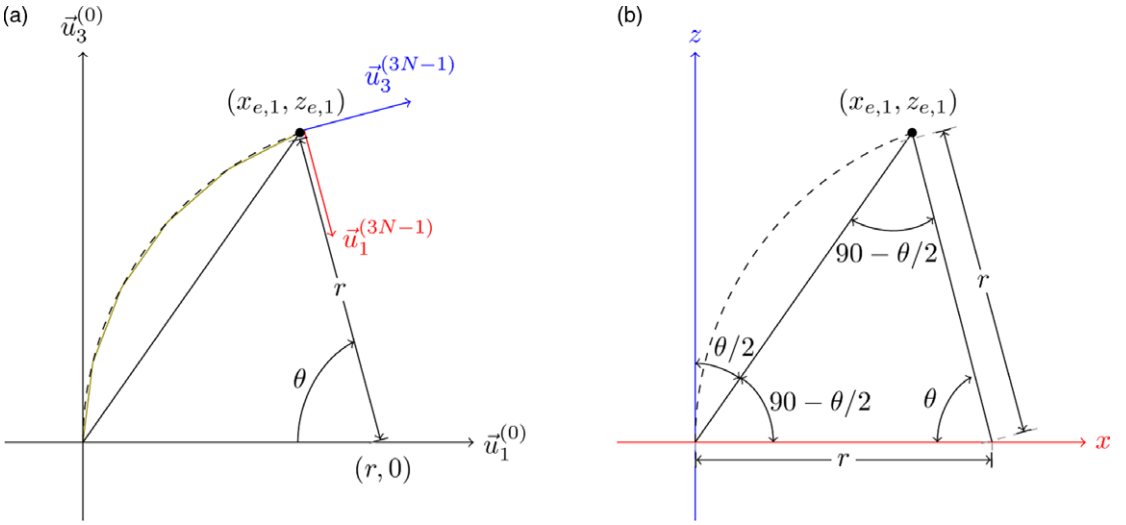

Figure 5. *Geometrical representation of the PCC approach for a single segment. (a) Soft robot as represented with discrete sections. Here, $\vec{u}_1^{(0)}$ represents the unit vector along the x-axis, $\vec{u}_3^{(0)}$ represents the unit vector along the z-axis of the base frame F_0, $\vec{u}_1^{(3N-1)}$ represents the unit vector along the x-axis, and $\vec{u}_3^{(3N-1)}$ represents the unit vector along the z-axis of the frame F_{3N-1}. (b) The definition of the polar angle (the angle from the z-axis to the line connecting the tip point to the origin) (adapted from [18]).*

frame F_0, shown in Fig. 5a, are used to construct a rigid-link representation of the soft robot with the same tip frame as the actual soft robot.

To obtain ten sections in equal lengths, the curve is divided into 11 uniformly spaced points and denoted with $x_{s,k}$, $y_{s,k}$, and $z_{s,k}$ parameters. These parameters are the tip-point position of the sth segment and kth section of the robot arm on the x, y, and z-axis. By using the tangent of these points, the bending angle of the arc $\theta_{i,s,k}$ and angle of the plane $\phi_{i,s,k}$ on the sth segment and kth section, and in total in each section for each segment, is acquired, presented in Eqs. (7)–(9), which results in a constant curvature arc representation of each segment. The arc length $\ell_{i,s,k}$ is obtained from the base frame to the tip-point position of each section, as presented in Eq. (9).

$$\theta_{i,s,k} = \text{atan2}\left(\left[(x_{s,k+1} - x_{s,k})^2 + (y_{s,k+1} - y_{s,k})^2\right]^{1/2}, (z_{s,k+1} - z_{s,k})\right) \tag{7}$$

$$\phi_{i,s,k} = \text{atan2}\left((y_{s,k+1} - y_{s,k}), (x_{s,k+1} - x_{s,k})\right) \tag{8}$$

$$\ell_{i,s,k} = \left[(x_{s,k+1} - x_{s,k})^2 + (y_{s,k+1} - y_{s,k})^2 + (z_{s,k+1} - z_{s,k})^2\right]^{1/2} \tag{9}$$

3.3. Kinematic modeling with Denavit-Hartenberg parameters

The discretized geometrical representation of a soft robot arm is illustrated in Fig. 6. The soft robot arms are modeled with segments having 10 sections with 3-DoF that are assembled on top of each other. As a consequence, each segment of the soft robot arm is represented with 30-DoF hyper-redundant rigid-link robot arm.

$\zeta_{i,s,k}$, $s_{i,s,k}$, $\gamma_{i,s,k}$, and $a_{i,s,k}$ parameters denote relative rotation of links, effective link length, twist angle, and relative offset of the link, respectively. In each section, the relative rotation between the 1st and 2nd links $\{\zeta_{i,s,2}, \zeta_{i,s,5}, \ldots, \zeta_{i,s,3N-1}\}$ is equal to the corresponding bending angle of the arc parameter $\{\theta_{i,s,1}, \theta_{i,s,2}, \ldots, \theta_{i,s,N}\}$. The relative rotation between the last joint of the previous section and the first joint of the following section $\{\zeta_{i,s,1}, \zeta_{i,s,4}, \ldots, \zeta_{i,s,3N-2}\}$ is equal to the corresponding angle of the plane

https://doi.org/10.1017/S026357472300139X Published online by Cambridge University Press

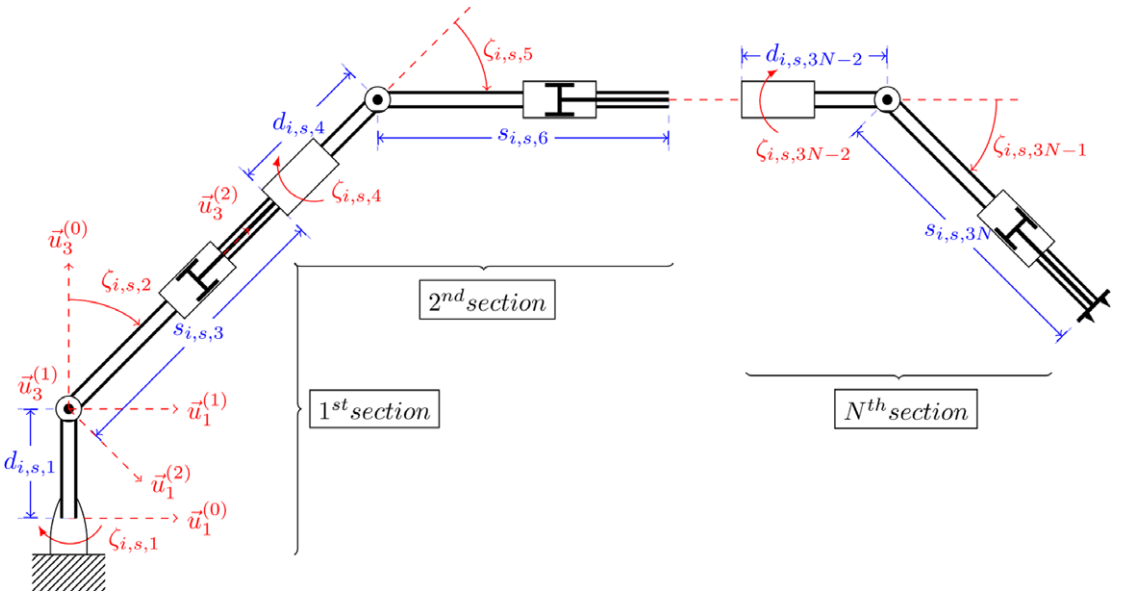

Figure 6. *The architecture of the robot arm.*

parameters $\{\phi_{i,s,1}, \phi_{i,s,2}, \ldots, \phi_{i,s,N}\}$. The PCC approach represents the soft arm as an arc on a plane that is rotated by an angle of ϕ. Therefore, only the first section of a segment is used to represent the rotation of the plane $\zeta_{i,s,1} = \phi_{i,s}$ and the rest maintains to be zero $\{\zeta_{i,s,4}, \zeta_{i,s,7}, \ldots, \zeta_{i,s,3N-2}\} = 0$. The effective link length parameter in each section $\{s_{i,s,3}, s_{i,s,6}, \ldots, s_{i,s,3N}\}$is equal to the corresponding arc length parameters $\{\ell_{i,s,1}, \ell_{i,s,2}, \ldots, \ell_{i,s,N}\}$. These parameters are presented in Table I with numerical values and their operating ranges, where N is equal to the total number of sections of the corresponding arm's one segment (i.e., $N = 10$ in our study). The limitations of each parameter are denoted in a way that each soft arm's PCC parameter θ does not exceed $\pi/2$ radians and ϕ does not exceed 2π radians. Since the material selected is almost incompressible, the range of the arc length is limited to $\ell_{i,s,\min} = 580$ mm and $\ell_{i,s,\max} = 600$ mm for a single-segment arm and $\ell_{i,s,\min} = 290$ mm and $\ell_{i,s,\max} = 300$ mm for a two-segment arm. The ranges of motion for all joints of the arms, given in Table I, can be updated for different materials that are used for producing the soft limbs by considering the material characteristics.

In order to manipulate and navigate the virtual soft arm model, necessary equations for forward and inverse kinematics of the robotic arms that represent soft arms are derived by using the Denavit-Hartenberg parameters. The tip-point position $\bar{p}_{i,s}$ of a single segment and transformation matrix $\hat{C}_{i,s}$ between coordinate frames F_0 and F_{3N-1} are given in Eqs. (10) and (11).

$$\bar{p}_{i,s} = d_{i,s,1}\bar{u}_3 + s_{i,s,3}\hat{C}_i^{(0,2)}\bar{u}_3 + d_{i,s,4}\hat{C}_i^{(0,3)}\bar{u}_3 + s_{i,s,6}\hat{C}_i^{(0,5)}\bar{u}_3 + \ldots + d_{i,s,3N-2}\hat{C}_i^{(0,3N-3)}\bar{u}_3 + s_{i,s,3N}\hat{C}_i^{(0,3N-1)}\bar{u}_3 \tag{10}$$

$$\hat{C}_{i,s} = e^{\tilde{u}_3\zeta_{i,s,1}}e^{-\tilde{u}_1\pi/2}e^{\tilde{u}_3\zeta_{i,s,2}}e^{\tilde{u}_1\pi/2}e^{\tilde{u}_3\zeta_{i,s,4}}e^{-\tilde{u}_1\pi/2}e^{\tilde{u}_3\zeta_{i,s,5}}e^{\tilde{u}_1\pi/2} \ldots e^{\tilde{u}_3\zeta_{i,s,3N-1}}e^{\tilde{u}_1\pi/2} \tag{11}$$

$\bar{p}_{i,s}$ and $\hat{C}_{i,s}$ equations can be further simplified as given in Eqs. (12) and (13). Here, $\vec{u}_i^{(k)}$ is defined as the i^{th} unit vector of frame F_k and $\bar{u}_i^{(k/j)}$ defines the resolution of $\vec{u}_i^{(k)}$ vector in the j^{th} frame F_j.

https://doi.org/10.1017/S026357472300139X Published online by Cambridge University Press

Table I. *Denavit-Hartenberg parameters of a single segment.*

Section#	Link#	$\zeta_{i,s}$ (rad)	$s_{i,s}$ (mm)	$\gamma_{i,s}$ (rad)	$a_{i,s}$ (mm)
#1	#1	$-\pi \leq \zeta_{i,s,1} \leq \pi$	$d_{i,s,1} = 0$	$-\pi/2$	–
	#2	$-\pi/20 \leq \zeta_{i,s,2} \leq \pi/20$	–	$\pi/2$	–
	#3	–	$\frac{\ell_{i,s,\min}}{10} \leq s_{i,s,3} \leq \frac{\ell_{i,s,\max}}{10}$	–	–
#2	#4	$\zeta_{i,s,4} = 0$	$d_{i,s,4} = 0$	$-\pi/2$	–
	#5	$-\pi/20 \leq \zeta_{i,s,5} \leq \pi/20$	–	$\pi/2$	–
	#6	–	$\frac{\ell_{i,s,\min}}{10} \leq s_{i,s,6} \leq \frac{\ell_{i,s,\max}}{10}$	–	–
⋮	⋮	⋮	⋮	⋮	⋮
#N	#3N-2	$\zeta_{i,s,3N-2} = 0$	$d_{i,s,3N-2} = 0$	$-\pi/2$	–
	#3N-1	$-\pi/20 \leq \zeta_{i,s,3N-1} \leq \pi/20$	–	$\pi/2$	–
	#3N	–	$\frac{\ell_{i,s,\min}}{10} \leq s_{i,s,3N} \leq \frac{\ell_{i,s,\max}}{10}$	–	–

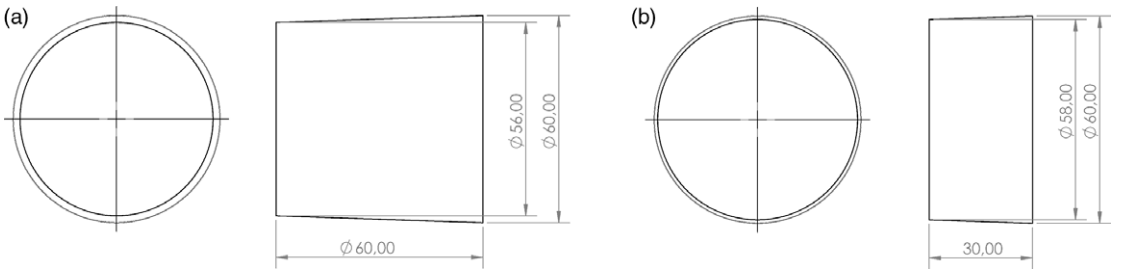

Figure 7. *The section architecture of a segment of the soft robotic arms: (a) the first section of the camera arm with one segment, (b) the first section of the grasper arm with two segments (all dimensions are in mm).*

$$\bar{p}_{i,s} = d_{i,s,1}\bar{u}_3 + s_{i,s,3}\bar{u}_3^{(2/0)} + d_{i,s,4}\bar{u}_3^{(3/0)} + s_{i,s,6}\bar{u}_3^{(5/0)} + \ldots + d_{i,s,3N-2}\bar{u}_3^{(3N-3/0)} + s_{i,s,3N}\bar{u}_3^{(3N-1/0)} \tag{12}$$

$$\hat{C}_{i,s} = e^{\tilde{u}_3\zeta_{i,s,1}} e^{\tilde{u}_2\zeta_{i,s,2}} e^{\tilde{u}_3\zeta_{i,s,4}} e^{\tilde{u}_2\zeta_{i,s,5}} \ldots e^{\tilde{u}_3\zeta_{i,s,3N-2}} e^{\tilde{u}_2\zeta_{i,s,3N-1}} \tag{13}$$

4. Representing soft robots in rigid-simulation environment

The representation of URSULA's soft limbs is designed as a combination of rigid bodies representing an RRP manipulator for each section in SolidWorks© software. Then, this model is transferred to the V-Realm Builder editor [22] in order to adjust the virtual representation and virtual environment consisting of obstacles and background images. The model is then used in MATLAB simulation via the VR Sink block available under the Simulink 3D Animation toolbox. This procedure is defined in detail as follows:

1. The CAD model of the soft robot is designed in SolidWorks© software. Two equally sized links are placed nested to form a section, presented in Fig. 7. Ten discrete sections are mounted on top of each other to form a segment. Two-segment grasper and palpation arms are formed with two segments mounted on top of each other.
2. The CAD design is exported in VRML file format to be edited in the V-Realm Builder editor.

https://doi.org/10.1017/S026357472300139X Published online by Cambridge University Press

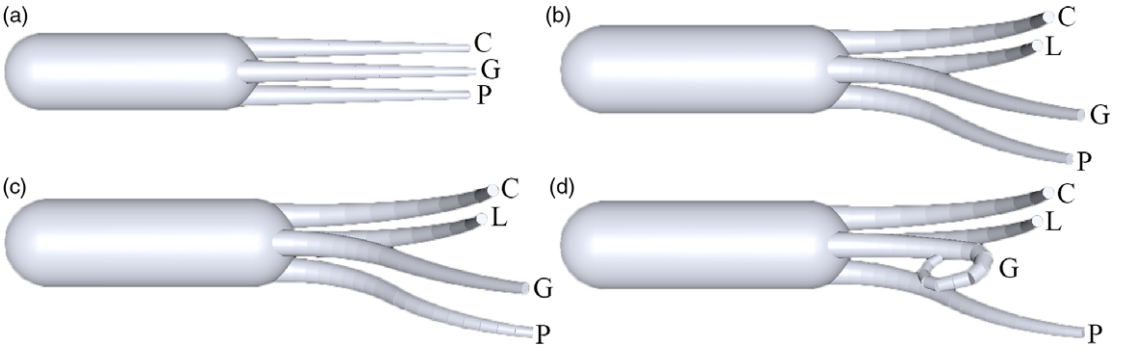

Figure 8. *Manipulation of the soft arms: (a) Initial condition: with maximum elongation and no bending of the arms; (b) Bending of single- and two-segment arms; (c) Elongation of the palpation arm: the elongation achieved can be observed by comparing the position of the palpation arm with respect to the grasper arm presented in (b); and (d) Grasping motion of the grasper arm: the second segment of the grasper arm is modified to achieve increased bending for grasping tasks.*

3. The discrete sections are defined as children of each other in the V-Realm Builder editor from the first section to the last section of each arm, which defines each section's motion as dependent on the previous section's motion.
4. To imitate the actual tasks of each arm, a viewpoint is mounted at the tip point of the camera arm and a spotlight is placed at the tip point of the light arm. Consequently, these are added as children of the last section of the arms.

At the end of this process, the virtually created rigid-link hyper-redundant robot represents the proposed design of the soft robot prototype. The tasks of each arm are performed on the developed simulation. Figure 8 presents the virtual representation of soft limbs created by sections that are composed of rigid-body models; in the initial condition without any bending or elongation (Fig. 8a), with bending of all segments of the arms (Fig. 8b), with reaching out of the palpation arm (Fig. 8c), and with bending of the grasper arm's second segment (Fig. 8d).

4.1. Verification of the kinematic representation

The accuracy of the representation is investigated through the comparison of tip-point positions and orientation calculated by using both forward kinematics formulations represented in Eqs. (10) and (11) and the quarter circle equation that is used to derive the PCC parameters. To validate that the presented modeling approach is suitable for this simulation, the following equations must satisfy each other: (1) The tip-point position calculation method given in Eq. (12) and the results of the curve equations presented in Eqs. (1)–(6), and (2) The orientation of the limb end calculation presented in Eqs. (13) and (20).

$$\bar{p}_{i,s} = p_{i,s,1}\bar{u}_1 + p_{i,s,2}\bar{u}_2 + p_{i,s,3}\bar{u}_3 \tag{14}$$

$$p^*_{i,s,1} = -r_1 \cos(\theta) + r_1 \tag{15}$$

$$p_{i,s,1} = p^*_{i,s,1} \cos(\phi) \tag{16}$$

$$p_{i,s,2} = p^*_{i,s,1} \sin(\phi) \tag{17}$$

$$p_{i,s,3} = r_1 \sin(\theta) \tag{18}$$

https://doi.org/10.1017/S026357472300139X Published online by Cambridge University Press

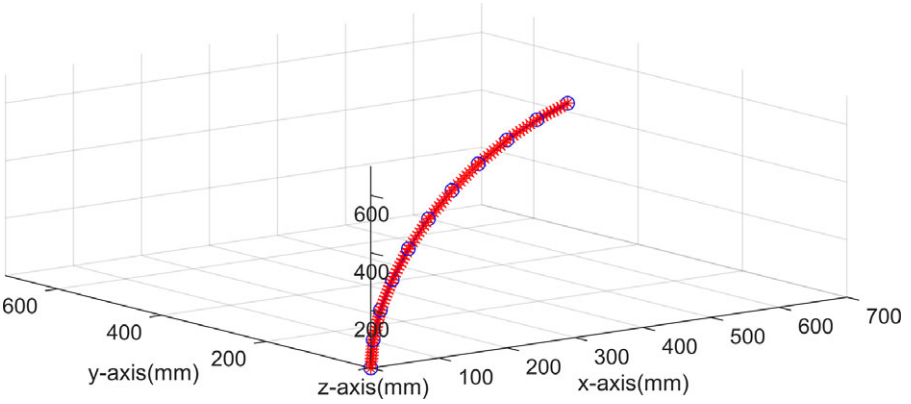

Figure 9. *Discretization of a single-segment arm.*

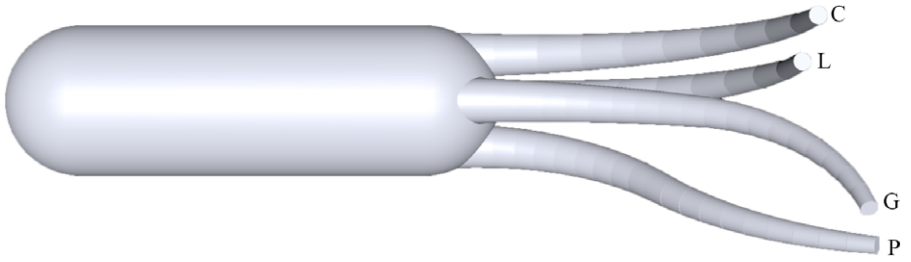

Figure 10. *Manipulation of the soft arms with different parameters.*

$$\hat{C}_{i,s}^{(0,N-1)} = [\bar{u}_1^{(N-1/0)} \bar{u}_2^{(N-1/0)} \bar{u}_3^{(N-1/0)}] \tag{19}$$

$$\hat{C}_{i,s}^{(0,N-1)} = \begin{bmatrix} \cos(\theta)\cos(\phi) & -\sin(\phi) & \sin(\theta)\cos(\phi) \\ \cos(\theta)\sin(\phi) & \cos(\phi) & \sin(\theta)\sin(\phi) \\ -\sin(\theta) & 0 & \cos(\theta) \end{bmatrix} \tag{20}$$

The validation process is carried out for the camera arm with one segment. Figure 9 represents the comparison of the positions of each discrete section for a single-segment arm with $\theta = 45°$ and $\phi = 30°$. The corresponding DH values of each section's parameters are as follows: $\bar{\zeta}_i = [30\ 4.5\ 0\ 0\ 9\ 0\ 0\ 9\ 0 \ldots 0\ 9\ 0]^T$, $\bar{s}_i = [0\ 0\ 60\ 0\ 0\ 60 \ldots 0\ 0\ 0]^T$, where the unit of $\bar{\zeta}_i$ values are given in degrees, and $\bar{s}_i$ are given in millimeters. The location of blue circles is obtained from the curve equation by dividing it into 10 equal lengths. The red points represent the section positions acquired by the DH parameters.

In addition to the visual representation of the validation through Fig. 9, the tip-point position and orientation of the camera arm obtained by the forward kinematics and the corresponding PCC parameters are related to each other via Eqs. (14)–(20). By comparing the results of these equations for different θ, ϕ, and ℓ parameters, a perfect match of the tip-point position and limb end orientation acquired by the Denavit-Hartenberg parameters and the PCC approach is observed.

The illustration with different values of θ, ϕ, and ℓ is given in Fig. 10. The camera arm is manipulated with $\theta = 90°$, $\phi = -5°$, and $\ell = 0$ mm, while the grasper arm's segments are manipulated with $\theta = 30°$, $\phi = 10°$, and $\ell = 10$ mm for segment 1, $\theta = 60°$, $\phi = 30°$, and $\ell = 10$ mm for segment 2, and palpation arm is manipulated with $\theta = 60°$, $\phi = 20°$, and $\ell = 0$ mm for segment 1, $\theta = -30°$, $\phi = 15°$, and $\ell = 0$ mm for segment 2.

https://doi.org/10.1017/S026357472300139X Published online by Cambridge University Press

5. Conclusions

This paper presents a procedure to visually represent the motion of a soft robot arm by using a simulation environment that is designed for rigid-body systems. The PCC approach is used to represent the motion of this soft robot arm. The initial assumption is that the position and posture of the soft robot are known or transmitted to the simulation environment. The methods of obtaining this information are not discussed here and are not in the scope of this paper. Another assumption is that the shape of the soft robot can be optimally represented by the PCC approach. We base our assumption on a recent study in [11]. Hence, the only validation we seek is in the kinematics domain. The PCC-based representation is discretized into multiple sections that are developed as 3-DoF robot arms. Consequently, the visual representation of a hyper-redundant robot arm is substituted to represent the motion of a soft robot arm. The kinematic model of this approach is verified through simulations. Also, the visual characteristics of the soft robot are imitated. To enhance the representation accuracy of the soft robot, the number of sections for a segment can be further increased.

The significance of this work is that it proposes a new method for visual representation of soft robot arms in graphical simulation environments developed for rigid-body systems. These simulation environments are generally optimal for running real-time operations. In the current setting, using a laptop computer with a Core i7 10th generation processor, 16 GB RAM capacity, and MATLAB Desktop Real-Time option, it was possible to run the simulation at 1 kHz sampling frequency and the virtual representation of the soft arms at 50 Hz. The obtained results are found to be sufficient yet can be improved with increased capacities of hardware [17]. An immediate application of the proposed simulation framework is model-mediated teleoperation. The continuation of this work involves the testing and verification of the model-mediated teleoperation system to control the soft limbs of the underwater biomimetic squid robot in laboratory and real-life experiments.

Author contributions. Prof. Berke Gür (BG) and Prof. Can Dede (CD) propose the idea of a novel biomimetic soft robot design with multiple tentacles. BG performed the design. Hazal Emet (HE) and CD constructed the kinematic structure. HE performed the simulation and tests, and CD supervised the simulation and tests. HE and BG wrote the first draft, and CD and BG provided draft revisions and supervision.

Financial support. This study is funded by The Scientific and Technological Research Council of Turkey (TÜBİTAK) with the project name Robotic Squid for Under-water Manipulation and Intervention and grant numbers 216M201 and 216M219.

Competing interests. The authors declare no competing interests exist.

Ethical approval. Not applicable.

Acknowledgments. We would like to thank the members of IZTECH Robotics Lab and RAML for helping with the activities.

Supplementary material. The supplementary material for this article can be found at https://doi.org/10.1017/S026357472300139X

References

[1] N. Williams, "Environmental credit crunch," *Curr. Biol.* **18**(21), R979–R980 (2008).
[2] A. Bleicher, "The gulf spill's lessons for robotics," *IEEE Spectr.* **47**(8), 9–11 (2010).
[3] B. A. Jones and I. D. Walker, "Kinematics for multisection continuum robots," *IEEE Trans. Robot.* **22**(1), 43–55 (2006).
[4] B. A. Jones and I. D. Walker, "Practical kinematics for real-time implementation of continuum robots," *IEEE Trans. Robot.* **22**(6), 1087–1099 (2006).
[5] M. Cianchetti, M. Calisti, L. Margheri, M. Kuba and C. Laschi, "Bioinspired locomotion and grasping in water: The soft eight-arm octopus robot," *Bioinspir. Biomim.* **10**(3), 035003 (2015).
[6] J. Fras, Y. Noh, M. Macias, H. Wurdemann and K. Althoefer, "Bio-inspired Octopus Robot Based on Novel Soft Fluidic Actuator," **In:** *2018 IEEE International Conference on Robotics and Automation (ICRA)* (IEEE, 2018) pp. 1583–1588.
[7] C. Christianson, Y. Cui, M. Ishida, X. Bi, Q. Zhu, G. Pawlak and M. T. Tolley, "Cephalopod-inspired robot capable of cyclic jet propulsion through shape change," *Bioinspir. Biomim.* **16**(1), 016014 (2020).

[8] R. K. Katzschmann, C. D. Santina, Y. Toshimitsu, A. Bicchi and D. Rus, "Dynamic Motion Control of Multi-segment Soft Robots Using Piecewise Constant Curvature Matched with an Augmented Rigid Body Model," **In:** *2019 2nd IEEE International Conference on Soft Robotics (RoboSoft)* (IEEE, 2019) pp. 454–461.
[9] C. D. Santina, A. Bicchi and D. Rus, "On an improved state parametrization for soft robots with piecewise constant curvature and its use in model based control," *IEEE Robot. Autom. Lett.* **5**(2), 1001–1008 (2020).
[10] L. Weerakoon and N. Chopra, "Bilateral Teleoperation of Soft Robots Under Piecewise Constant Curvature Hypothesis: An Experimental Investigation," **In:** *2020 American Control Conference (ACC)* (IEEE, 2020) pp. 2124–2129.
[11] H. Cheng, H. Liu, X. Wang and B. Liang, "Approximate Piecewise Constant Curvature Equivalent Model and Their Application to Continuum Robot Configuration Estimation," **In:** *2020 IEEE International Conference on Systems, Man, and Cybernetics (SMC)* (IEEE, 2020) pp. 1929–1936.
[12] J. Till, V. Aloi and C. Rucker, "Real-time dynamics of soft and continuum robots based on cosserat rod models," *Int. J. Robot. Res.* **38**(6), 723–746 (2019).
[13] A. A. Alqumsan, S. Khoo and M. Norton, "Robust control of continuum robots using cosserat rod theory," *Mech. Mach. Theory* **131**, 48–61 (2019).
[14] F. Janabi-Sharifi, A. Jalali and I. D. Walker, "Cosserat rod-based dynamic modeling of tendon-driven continuum robots: A tutorial," *IEEE Access* **9**, 68703–68719 (2021).
[15] A. Martin-Barrio, S. Terrile, M. Diaz-Carrasco, J. del Cerro and A. Barrientos, "Modelling the soft robot kyma based on real-time finite element method," *Comput. Graph. Forum* **39**(6), 289–302 (2020).
[16] E. Coevoet, T. Morales-Bieze, F. Largilliere, Z. Zhang, M. Thieffry, M. Sanz-Lopez, B. Carrez, D. Marchal, O. Goury, J. Dequidt and C. Duriez, "Software toolkit for modeling, simulation, and control of soft robots," *Adv. Robot.* **31**(22), 1208–1224 (2017).
[17] F. Largilliere, V. Verona, E. Coevoet, M. Sanz-Lopez, J. Dequidt and C. Duriez, "Real-Time Control of Soft-Robots Using Asynchronous Finite Element Modeling," **In:** *2015 IEEE International Conference on Robotics and Automation (ICRA)* (IEEE, 2015) pp. 2550–2555.
[18] R. J. Webster III and B. A. Jones, "Design and kinematic modeling of constant curvature continuum robots: A review," *Int. J. Robot. Res.* **29**(13), 1661–1683 (2010).
[19] F. Renda, V. Cacucciolo, J. Dias and L. Seneviratne, "Discrete Cosserat Approach for Soft Robot Dynamics: A New Piece-Wise Constant Strain Model with Torsion and Shears," **In:** *2016 IEEE/RSJ International Conference on Intelligent Robots and Systems (IROS)* (IEEE, 2016) pp. 5495–5502.
[20] Z. Zhang, J. Dequidt, A. Kruszewski, F. Largilliere and C. Duriez, "Kinematic Modeling and Observer Based Control of Soft Robot Using Real-Time Finite Element Method," **In:** *2016 IEEE/RSJ International Conference on Intelligent Robots and Systems (IROS)* (IEEE, 2016) pp. 5509–5514.
[21] E. Uzunoğlu and M. I. C. Dede, "Extending model-mediation method to multi-degree-of-freedom teleoperation systems experiencing time delays in communication," *Robotica* **35**(5), 1121–1136 (2017).
[22] N. Khaled, *Virtual Reality and Animation for MATLAB® and Simulink® Users: Visualization of Dynamic Models and Control Simulations* (Springer, London, 2012).

Cite this article: H. Emet, B. Gür and M. İ. C. Dede (2024). "The design and kinematic representation of a soft robot in a simulation environment", Robotica **42**, 139–152. https://doi.org/10.1017/S026357472300139X